









TECH BRIEFS

NATIONAL AERONAUTICS AND SPACE ADMINISTRATION

-  **Technology Focus**
-  **Electronics/Computers**
-  **Software**
-  **Materials**
-  **Mechanics**
-  **Machinery/Automation**
-  **Manufacturing**
-  **Bio-Medical**
-  **Physical Sciences**
-  **Information Sciences**
-  **Books and Reports**

INTRODUCTION

Tech Briefs are short announcements of innovations originating from research and development activities of the National Aeronautics and Space Administration. They emphasize information considered likely to be transferable across industrial, regional, or disciplinary lines and are issued to encourage commercial application.

Availability of NASA Tech Briefs and TSPs

Requests for individual Tech Briefs or for Technical Support Packages (TSPs) announced herein should be addressed to

National Technology Transfer Center

Telephone No. (800) 678-6882 or via World Wide Web at www2.nttc.edu/leads/

Please reference the control numbers appearing at the end of each Tech Brief. Information on NASA's Commercial Technology Team, its documents, and services is also available at the same facility or on the World Wide Web at www.nctn.hq.nasa.gov.

Commercial Technology Offices and Patent Counsels are located at NASA field centers to provide technology-transfer access to industrial users. Inquiries can be made by contacting NASA field centers and program offices listed below.

NASA Field Centers and Program Offices

Ames Research Center

Carolina Blake
(650) 604-1754
carolina.m.blake@nasa.gov

Dryden Flight Research Center

Jenny Baer-Riedhart
(661) 276-3689
jenny.baer-riedhart@dfrc.nasa.gov

Goddard Space Flight Center

Nona Cheeks
(301) 286-5810
Nona.K.Cheeks.1@gssc.nasa.gov

Jet Propulsion Laboratory

Art Murphy, Jr.
(818) 354-3480
arthur.j.murphy-jr@jpl.nasa.gov

Johnson Space Center

Charlene E. Gilbert
(281) 483-3809
commercialization@jsc.nasa.gov

Kennedy Space Center

Jim Aliberti
(321) 867-6224
Jim.Aliberti-1@ksc.nasa.gov

Langley Research Center

Jesse Midgett
(757) 864-3936
jesse.c.midgett@nasa.gov

John H. Glenn Research Center at Lewis Field

Larry Viterna
(216) 433-3484
cto@grc.nasa.gov

Marshall Space Flight Center

Vernotto McMillan
(256) 544-2615
vernotto.mcmillan@msfc.nasa.gov

Stennis Space Center

Robert Bruce
(228) 688-1929
robert.c.bruce@nasa.gov

NASA Program Offices

At NASA Headquarters there are seven major program offices that develop and oversee technology projects of potential interest to industry:

Carl Ray

Small Business Innovation Research Program (SBIR) & Small Business Technology Transfer Program (STTR)
(202) 358-4652 or
cray@mail.hq.nasa.gov

Benjamin Neumann

Innovative Technology Transfer Partnerships (Code RP)
(202) 358-2320
benjamin.j.neumann@nasa.gov

John Mankins

Office of Space Flight (Code MP)
(202) 358-4659 or
jmankins@mail.hq.nasa.gov

Terry Hertz

Office of Aero-Space Technology (Code RS)
(202) 358-4636 or
thertz@mail.hq.nasa.gov

Glen Mucklow

Office of Space Sciences (Code SM)
(202) 358-2235 or
gmucklow@mail.hq.nasa.gov

Roger Crouch

Office of Microgravity Science Applications (Code U)
(202) 358-0689 or
rcrouch@hq.nasa.gov

Granville Paules

Office of Mission to Planet Earth (Code Y)
(202) 358-0706 or
gpaules@mtpe.hq.nasa.gov



TECH BRIEFS

NATIONAL AERONAUTICS AND SPACE ADMINISTRATION



5 Technology Focus:

- 5 Advanced Signal Conditioners for Data-Acquisition Systems
- 5 Downlink Data Multiplexer
- 6 Viewing ISS Data in Real Time via the Internet
- 7 Autonomous Environment-Monitoring Networks
- 8 Readout of DSN Monitor Data



9 Electronics/Computers

- 9 Parallel-Processing Equalizers for Multi-Gbps Communications
- 10 AIN-Based Packaging for SiC High-Temperature Electronics

11 Software



- 11 Software for Optimizing Quality Assurance of Other Software
- 11 The TechSat 21 Autonomous Sciencecraft Experiment
- 11 Software for Analyzing Laminar-to-Turbulent Flow Transitions



13 Materials

- 13 Elastomer Filled With Single-Wall Carbon Nanotubes



15 Mechanics

- 15 Modifying Ship Air-Wake Vortices for Aircraft Operations
- 16 Strain-Gauge Measurement of Weight of Fluid in a Tank
- 16 Advanced Docking System With Magnetic Initial Capture



19 Machinery/Automation

- 19 Blade-Pitch Control for Quieting Tilt-Rotor Aircraft
- 20 Solar Array Panels With Dust-Removal Capability



21 Manufacturing

- 21 Aligning Arrays of Lenses and Single-Mode Optical Fibers
- 22 Automatic Control of Arc Process for Making Carbon Nanotubes
- 22 Curved-Focal-Plane Arrays Using Deformed-Membrane Photodetectors



25 Physical Sciences

- 25 Role of Meteorology in Flights of a Solar-Powered Airplane
- 26 Model of Mixing Layer With Multicomponent Evaporating Drops
- 27 Solution-Assisted Optical Contacting



29 Information Sciences

- 29 Improved Discrete Approximation of Laplacian of Gaussian
- 30 Utilizing Expert Knowledge in Estimating Future STS Costs



31 Books & Reports

- 31 Study of Rapid-Regression Liquefying Hybrid Rocket Fuels
- 31 More About the Phase-Synchronized Enhancement Method

This document was prepared under the sponsorship of the National Aeronautics and Space Administration. Neither the United States Government nor any person acting on behalf of the United States Government assumes any liability resulting from the use of the information contained in this document, or warrants that such use will be free from privately owned rights.

Advanced Signal Conditioners for Data-Acquisition Systems

“Smart” circuitry repairs itself by switching in spare parts as needed.

John F. Kennedy Space Center, Florida

Signal conditioners embodying advanced concepts in analog and digital electronic circuitry and software have been developed for use in data-acquisition systems that are required to be compact and lightweight, to utilize electric energy efficiently, and to operate with high reliability, high accuracy, and high power efficiency, without intervention by human technicians. These signal conditioners were originally intended for use aboard spacecraft. There are also numerous potential terrestrial uses — especially in the fields of aeronautics and medicine, wherein it is necessary to monitor critical functions.

Going beyond the usual analog and digital signal-processing functions of prior signal conditioners, the new signal conditioner performs the following additional functions:

- It continuously diagnoses its own electronic circuitry, so that it can detect failures and repair itself (as described below) within seconds.
- It continuously calibrates itself on the basis of a highly accurate and stable voltage reference, so that it can continue to generate accurate measurement data, even under extreme environmental conditions.
- It repairs itself in the sense that it contains a microcontroller that reroutes

signals among redundant components as needed to maintain the ability to perform accurate and stable measurements.

- It detects deterioration of components, predicts future failures, and/or detects imminent failures by means of a real-time analysis in which, among other things, data on its present state are continuously compared with locally stored historical data.
- It minimizes unnecessary consumption of electric energy.

The design architecture divides the signal conditioner into three main sections: an analog signal section, a digital module, and a power-management section. The design of the analog signal section does not follow the traditional approach of ensuring reliability through total redundancy of hardware: Instead, following an approach called “spare parts — tool box,” the reliability of each component is assessed in terms of such considerations as risks of damage, mean times between failures, and the effects of certain failures on the performance of the signal conditioner as a whole system. Then, fewer or more spares are assigned for each affected component, pursuant to the results of this analysis, in order to obtain the required degree of reliability of the signal conditioner as a whole system.

The digital module comprises one or more processors and field-programmable gate arrays, the number of each depending on the results of the aforementioned analysis. The digital module provides redundant control, monitoring, and processing of several analog signals. It is designed to minimize unnecessary consumption of electric energy, including, when possible, going into a low-power “sleep” mode that is implemented in firmware. The digital module communicates with external equipment via a personal-computer serial port. The digital module monitors the “health” of the rest of the signal conditioner by processing defined measurements and/or trends. It automatically makes adjustments to respond to channel failures, compensate for effects of temperature, and maintain calibration.

This work was done by Angel Lucena and Jose Perotti of Kennedy Space Center, and Anthony Eckhoff and Pedro Medelius of Dynacs, Inc. Further information is contained in a TSP (see page 1).

This invention is owned by NASA, and a patent application has been filed. Inquiries concerning nonexclusive or exclusive license for its commercial development should be addressed to the Technology Programs and Commercialization Office, Kennedy Space Center, (321) 867-8130. Refer to KSC-12301.

Downlink Data Multiplexer

Bandwidth is allocated as needed among four data streams of various rates.

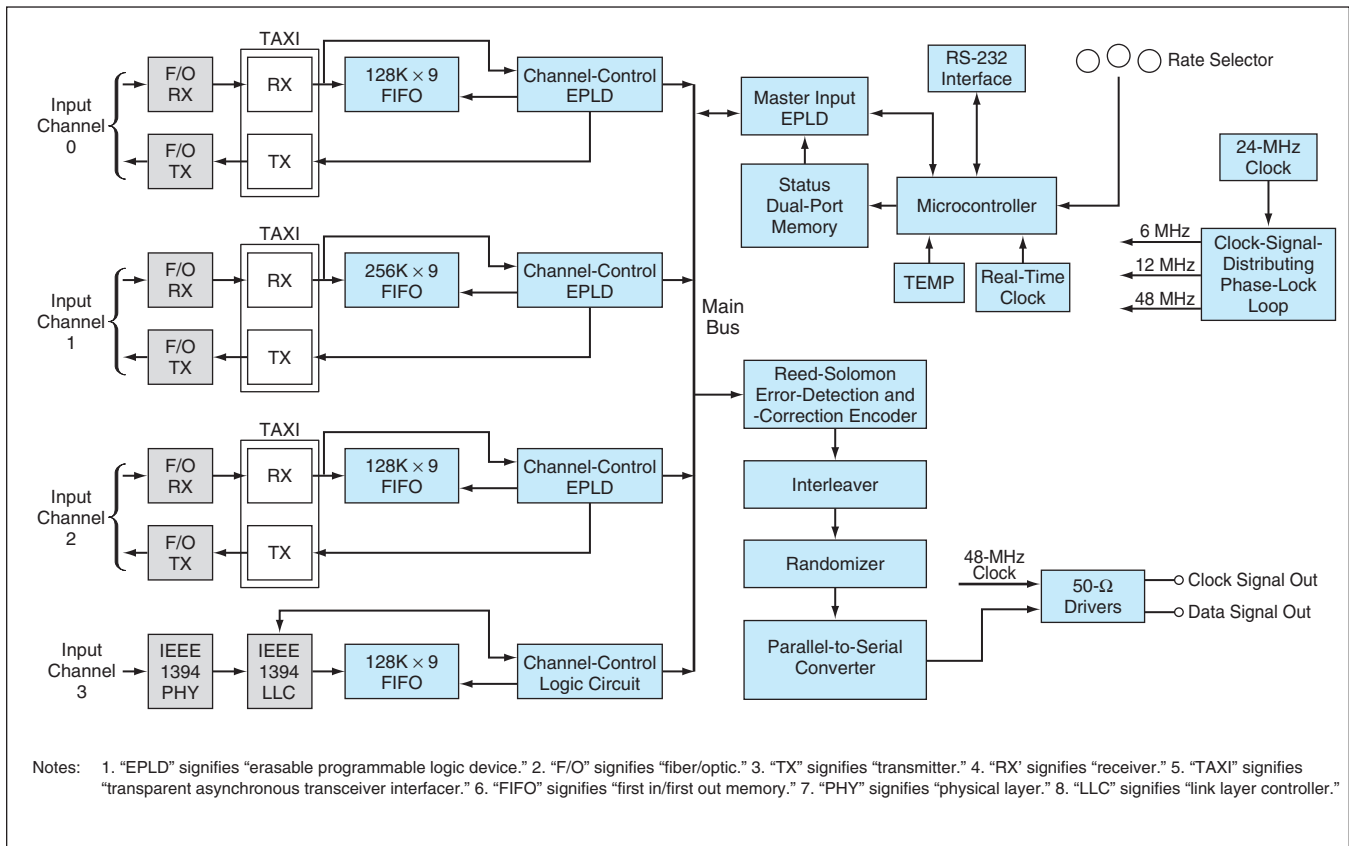
Lyndon B. Johnson Space Center, Houston, Texas

A multiplexer/demultiplexer system has been developed to enable the transmission, over a single channel, of four data streams generated by a variety of sources at different (including variable) bit rates. In the original intended application, replicas of this multiplexer/demultiplexer system would be incorporated into the spacecraft-to-ground communication systems of the space shuttles. The multiplexer of each system would be installed in the spacecraft, where it would acquire and process data

from such sources as commercial digital camcorders, video tape recorders, and the spacecraft telemetry system. The demultiplexer of each system would be installed in a ground station. Purely terrestrial systems of similar design could be attractive for use in situations in which there are requirements to transmit multiple streams of high-quality video data and possibly other data over single channels.

The figure is a block diagram of the multiplexer as configured to process

data received via three fiber-optic channels like those of the International Space Station and one electrical-cable channel that conforms to the Institute of Electrical and Electronic Engineers (IEEE) 1394 standard. (This standard consists of specifications of a high-speed serial data interface, the physical layer of which includes a cable known in the art as “FireWire.” An IEEE 1394 interface can also transfer power between the components to which it is connected.) The fiber-optic channels carry packet



This **Data Multiplexer** combines four input streams (three fiber-optic TAXI interface channels and one IEEE 1394 channel) into a single output stream.

and/or bit-stream signals that conform to the standards of the Consultative Committee for Space Data Systems (CCSDS). The IEEE 1394 interface accepts an isochronous signal like that from a digital camcorder or a video tape recorder.

The processing of the four input data streams to combine them into one output stream is governed by a statistical multiplexing algorithm that features a flow-control capability and makes it possible to utilize the transmission channel with nearly 100-percent efficiency. This algorithm allocates the available bandwidth of the transmission channel to the

data streams according to a combination of data rates and preassigned priorities. Incoming data streams that demand too much bandwidth are blocked. Bandwidth not needed for a transmission of a given data stream is allocated to other streams as available. Priority is given to the IEEE 1394 stream.

In addition to the four incoming data streams, the multiplexer transmits data on the status of the system. An operator can monitor and control the multiplexer via displays and controls on the multiplexer housing. The output of the multiplexer is connected via a coaxial cable with an impedance of 50 Ω to an

interface circuit compatible with the space-shuttle high-speed digital down-link, which operates at a rate of 48 Mb/s.

This work was done by S. Douglas Holland, Glen F. Steele, Denise M. Romero, and Robert David Koudelka of Johnson Space Center. Further information is contained in a TSP (see page 1).

This invention is owned by NASA, and a patent application has been filed. Inquiries concerning nonexclusive or exclusive license for its commercial development should be addressed to the Patent Counsel, Johnson Space Center, (281) 483-0837. Refer to MSC-23303.

Viewing ISS Data in Real Time via the Internet

Marshall Space Flight Center, Alabama

EZStream is a computer program that enables authorized users at diverse terrestrial locations to view, in real time, data generated by scientific payloads aboard the International Space Station (ISS). The only computation/communication resource needed for use of EZStream is a computer equipped with

standard Web-browser software and a connection to the Internet. EZStream runs in conjunction with the TReK software, described in a prior *NASA Tech Briefs* article, that coordinates multiple streams of data for the ground communication system of the ISS. EZStream includes server components that interact

with TReK within the ISS ground communication system and client components that reside in the users' remote computers. Once an authorized client has logged in, a server component of EZStream pulls the requested data from a TReK application-program interface and sends the data to the client. Future

EZStream enhancements will include (1) extensions that enable the server to receive and process arbitrary data streams on its own and (2) a Web-based graphical-user-interface-building sub-

program that enables a client who lacks programming expertise to create customized display Web pages.

This program was written by Gerry Myers and Jim Chamberlain of AZ Technology, Inc.,

for Marshall Space Flight Center. For further information, contact the company's New Technology Representative, David O'Neil, at (256) 837-9877. MFS-31836

Autonomous Environment-Monitoring Networks

These neural networks recognize novel features in streams of input data.

NASA's Jet Propulsion Laboratory, Pasadena, California

Autonomous environment-monitoring networks (AEMNs) are artificial neural networks that are specialized for recognizing familiarity and, conversely, novelty. Like a biological neural network, an AEMN receives a constant stream of inputs. For purposes of computational implementation, the inputs are vector representations of the information of interest. As long as the most recent input vector is similar to the previous input vectors, no action is taken. Action is taken only when a novel vector is encountered. Whether a given input vector is regarded as novel depends on the previous vectors; hence, the same input vector could be regarded as familiar or novel, depending on the context of previous input vectors. AEMNs have been proposed as means to enable exploratory robots on remote planets to recognize novel features that could merit closer scientific attention. AEMNs could also be useful for processing data from medical instrumentation for automated monitoring or diagnosis.

The primary substructure of an AEMN is called a spindle. In its simplest form, a spindle consists of a central vector (C), a scalar (r), and algorithms for changing C and r . The vector C is constructed from all the vectors in a given continuous

stream of inputs, such that it is minimally distant from those vectors. The scalar r is the distance between C and the most remote vector in the same set.

The construction of a spindle involves four vital parameters: setup size, spindle-population size, and the radii of two novelty boundaries. The setup size is the number of vectors that are taken into account before computing C . The spindle-population size is the total number of input vectors used in constructing the spindle — counting both those that arrive before and those that arrive after the computation of C . The novelty-boundary radii are distances from C that partition the neighborhood around C into three concentric regions (see Figure 1). During construction of the spindle, the changing spindle radius is denoted by h . It is the final value of h , reached before beginning construction on the next spindle, that is denoted by r .

During construction of a spindle, if a new vector falls between C and the inner boundary, the vector is regarded as completely familiar and no action is taken. If the new vector falls into the region be-

tween the inner and outer boundaries, it is considered unusual enough to warrant the adjustment of C and r by use of the aforementioned algorithms, but not unusual enough to be considered novel. If a vector falls outside the outer boundary, it is considered novel, in which case one of several appropriate responses could be initiation of construction of a new spindle.

An AEMN comprises a collection of spindles that represent a typical history or range of behaviors of a system that one seeks to monitor. An AEMN can be represented as a familiarity map, on which successive spindles are represented by adjacent circles that are added as construction proceeds. A familiarity map could be simple or complex, depending on the monitored system. For example, the range of behaviors of a complex system might be represented by a networklike familiarity map that could even include dead-end branches that lead to the demise of the system. An automated monitoring system based on the AEMN corresponding to the familiarity map could recognize that the system was

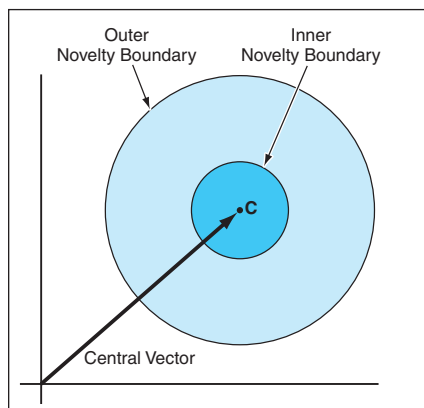


Figure 1. The Central Vector and The Novelty Boundaries play major roles in the construction of a spindle.

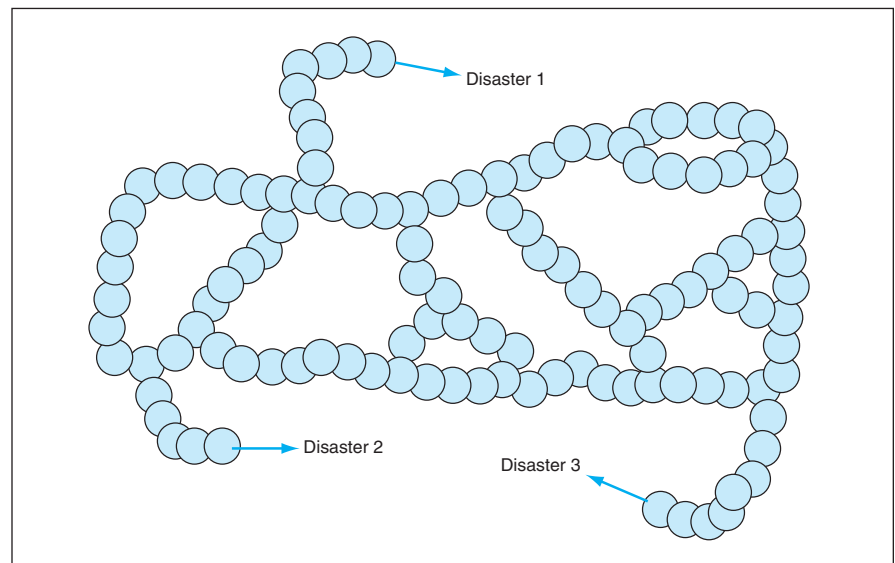


Figure 2. A Familiarity Map comprises a sequence of overlapping circles that represent spindles constructed from data acquired in observation or simulation of a system to be monitored.

progressing along a dead-end branch and respond by generating an alarm or triggering control action to move the system away from the dead-end condition.

This work was done by Charles Hand of Caltech for NASA's Jet Propulsion Laboratory. Further information is contained in a TSP (see page 1).

This software is available for commercial licensing. Please contact Don Hart of the California Institute of Technology at (818) 393-3425. Refer to NPO-30408.

● Readout of DSN Monitor Data

NASA's Jet Propulsion Laboratory, Pasadena, California

DSN Monitor Data Reader is a computer program that, as its name suggests, reads file of monitor data from the Deep Space Network (DSN). The monitor data constitute information on the status and performance of tracking, telemetry, command, and pointing equipment at the DSN antennas. The DSN has recently introduced a new, more advanced monitor data format, denoted 0158-Mon, that is based on the standard formatted data unit (SFDU) and compressed header

data objects (CHDO) of the Consultative Committee for Space Data Systems (CCSDS). The 0158-Mon data format is a very flexible generic format that provides for specific variable-length formats and for self-identifying parameters that obviate the proprietary NASA Communications (NASCOM) bit-packed formats of the past. The monitor data SFDUs are also encapsulated in Standard DSN Blocks and routed to DSN customers for processing at their local mission control

centers. This program helps a DSN customer to read and parse the monitor data to assess the statuses of the DSN stations in support of spacecraft flight operations.

This program was written by Katherine Levister and May Tran of Caltech for NASA's Jet Propulsion Laboratory. Further information is contained in a TSP (see page 1).

This software is available for commercial licensing. Please contact Don Hart of the California Institute of Technology at (818) 393-3425. Refer to NPO-30723.



Parallel-Processing Equalizers for Multi-Gbps Communications

One can compromise among computational efficiency, complexity of circuitry, and processing rates.

NASA's Jet Propulsion Laboratory, Pasadena, California

Architectures have been proposed for the design of frequency-domain least-mean-square complex equalizers that would be integral parts of parallel-processing digital receivers of multigigahertz radio signals and other quadrature-phase-shift-keying (QPSK) or 16-quadrature-amplitude-modulation (16-QAM) of data signals at rates of multiple gigabits per second. "Equalizers" as used here denotes receiver subsystems that compensate for distortions in the phase and frequency responses of the broad-band radio-frequency channels typically used to convey such signals. The proposed architectures are suitable for realization in very-large-scale integrated (VLSI) circuitry and, in particular, complementary metal oxide semiconductor (CMOS) application-specific integrated circuits (ASICs) operating at frequencies lower than modulation symbol rates.

A digital receiver of the type to which the proposed architecture applies (see Figure 1) would include an analog-to-digital converter (A/D) operating at a rate, f_s , of 4 samples per symbol period. To obtain the high speed necessary for sampling, the A/D and a 1:16 demultiplexer immediately following it would be constructed as GaAs integrated circuits. The parallel-processing circuitry downstream of the demultiplexer, including a demodulator followed by an equalizer, would operate at a rate of only $f_s/16$ (in other words, at 1/4 of the symbol rate). The output from the equalizer would be four parallel streams of in-phase (I) and quadrature (Q) samples.

The proposed architectures would implement subconvolution (see Figure 2), fast-Fourier-transform/inverse-fast-Fourier-transform (FFT-IDFT), and discrete-Fourier-transform/inverse-discrete-Fourier-transform (DFT-IDFT) overlap-and-save filter algorithms. A key property of the proposed architectures is that one can make engineering compromises among computational efficiency, complexity of circuitry, and processing rates. Such trades are made

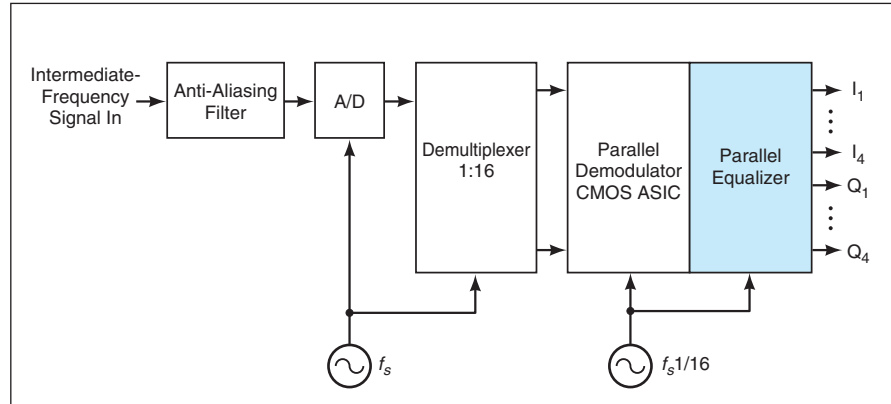


Figure 1. A Parallel-Processing Digital Receiver would include a parallel-processing equalizer.

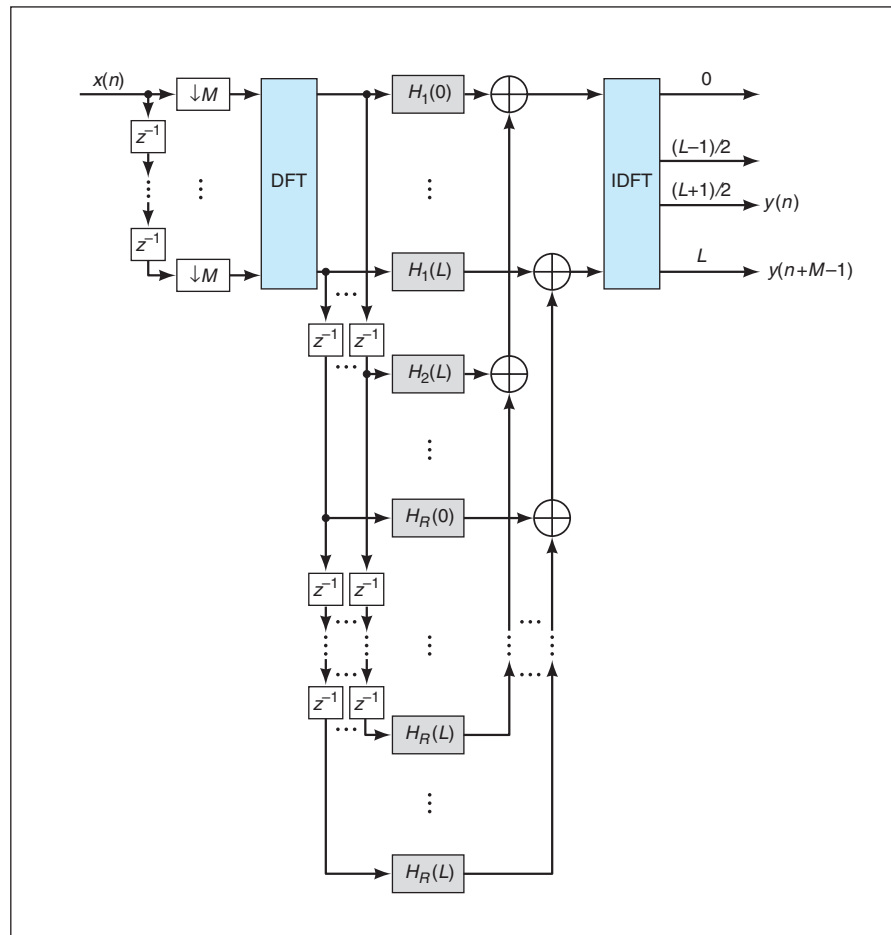


Figure 2. A Parallel Subconvolution Filter Bank would perform R subconvolutions, each of length $L+1$, at $1/M$ of the input sample rate. The symbol z^{-1} denotes a delay of one sample period, " $\downarrow 16$ " signifies decimation by a factor of 16, and H_i denotes a frequency-domain digital filter.

possible, in part, by utilizing subconvolutions and relatively simple digital signal-processing methods in such a manner as to eliminate a lower bound imposed on FFT-IFFT lengths by equalizer tap lengths. For a given receiver, the equalizer tap length would theoretically be unlimited, and the FFT-IFFT length could be chosen completely independently of the equalizer tap length. The FFT-IFFT length could be determined on the basis of the de-

sired reduction in the processing rate. The specific values chosen for the proposed architectures are an equalizer tap length of 32, with an FFT-IFFT length of 8 chosen to enable processing at 1/4 of the symbol rate.

This work was done by Andrew Gray, Parminder Ghuman, Scott Hoy, and Edgar H. Satorius of Caltech for NASA's Jet Propulsion Laboratory. Further information is contained in a TSP (see page 1).

In accordance with Public Law 96-517,

the contractor has elected to retain title to this invention. Inquiries concerning rights for its commercial use should be addressed to

Intellectual Assets Office

JPL

Mail Stop 202-233

4800 Oak Grove Drive

Pasadena, CA 91109

(818) 354-2240

E-mail: ipgroup@jpl.nasa.gov

Refer to NPO-30246, volume number and page number.

AIN-Based Packaging for SiC High-Temperature Electronics

Electronic packaging can withstand a continuous temperature of 500 °C.

John H. Glenn Research Center, Cleveland, Ohio

Packaging made primarily of aluminum nitride has been developed to enclose silicon carbide-based integrated circuits (ICs), including circuits containing SiC-based power diodes, that are capable of operation under conditions more severe than can be withstood by silicon-based integrated circuits. A major objective of this development was to enable packaged SiC electronic circuits to operate continuously at temperatures up to 500 °C. AIN-packaged SiC electronic circuits have commercial potential for incorporation into high-power electronic equipment and into sensors that must withstand high temperatures and/or high pressures in diverse applications that include exploration in outer space, well logging, and monitoring of nuclear power systems. This packaging embodies concepts drawn from flip-chip packaging of silicon-based integrated circuits. One or more SiC-based circuit chips are mounted on an aluminum nitride package substrate or sandwiched between two such substrates. Intimate electrical

connections between metal conductors on the chip(s) and the metal conductors on external circuits are made by direct bonding to interconnections on the package substrate(s) and/or by use of holes through the package substrate(s). This approach eliminates the need for wire bonds, which have been the most vulnerable links in conventional electronic circuitry in hostile environments. Moreover, the elimination of wire bonds makes it possible to pack chips more densely than was previously possible.

Especially notable components of packaging of this type are the following:

- AIN substrates that have high thermal conductivity [170 W/(m·K)] and a coefficient of thermal expansion (CTE) that matches that of SiC;
- Thick gold conductor film circuit traces, the adhesion and sheet resistance of which do not change measurably at 500 °C over time periods as long as 1,000 hours; and
- Glass passivation/sealing layers that have a breakdown potential of 2,575 V

at room temperature and, at 500 °C, breakdown potentials of 1,100 V for encapsulation of Au conductors and 1,585 V for encapsulation of Pt conductors.

The matching of CTEs minimizes thermal stresses. Packaging interconnections are monometallic or bimetallic and able to withstand high temperatures. These and other features are known to contribute to reliability at high temperatures and are expected to extend the high-temperature functionality of the packaged electronic devices. Further research will be necessary to characterize the long-term reliability of SiC-based circuits in AIN-based packages.

This work was done by Ender Savrun of Sienna Technologies, Inc., for Glenn Research Center. For further information, access <http://www.siennatech.com>.

Inquiries concerning rights for the commercial use of this invention should be addressed to NASA Glenn Research Center, Commercial Technology Office, Attn: Steve Fedor, Mail Stop 4-8, 21000 Brookpark Road, Cleveland, Ohio 44135. Refer to LEW-17478.

2 Software for Optimizing Quality Assurance of Other Software

Software assurance is the planned and systematic set of activities that ensures that software processes and products conform to requirements, standards, and procedures. Examples of such activities are the following: code inspections, unit tests, design reviews, performance analyses, construction of traceability matrices, etc. In practice, software development projects have only limited resources (e.g., schedule, budget, and availability of personnel) to cover the entire development effort, of which assurance is but a part. Projects must therefore select judiciously from among the possible assurance activities. At its heart, this can be viewed as an optimization problem; namely, to determine the allocation of limited resources (time, money, and personnel) to minimize risk or, alternatively, to minimize the resources needed to reduce risk to an acceptable level. The end result of the work reported here is a means to optimize quality-assurance processes used in developing software. This is achieved by combining two prior programs in an innovative manner:

- *First Program:* The first of these programs is the Advanced Risk Reduction Tool (ARRT), which can be used to calculate the costs and benefits of a set of assurance activities on a given software project. ARRT is itself based on a risk-management tool, Defect Detection and Prevention (DDP). DDP uses a detailed mathematical model of requirements, risks, and mitigations.
- *Second Program:* The second of these programs is the TAR2 “treatment learner,” which can be used to determine from a large set of factors those factor settings most critical to attaining a given objective.
- *Innovative Combination:* The major contribution of this work is the combination of these two programs. They are combined so as to operate in an iterative procedure, as follows: In each cycle of the iteration, TAR2 is tuned to identify the most critical software assurance activities, both those most critical to perform (because they contribute to cost-effective

risk reduction), and those most critical to not perform (because they detract from cost-effective risk reduction).

These identified activities are then set accordingly in ARRT, and the cost-benefit calculations rerun. Repeating this cycle determines more and more activities to perform (and/or to not perform), culminating in a solution that is (near) optimal. An important aspect of this approach is that it allows for human experts to add further guidance during each iteration of the cycle. For example, if the experts observe that two of the recommended activities are actually incompatible (say, because they would both require use of the same limited resource at the same time), they can reject the TAR2 recommendations involving this pair of activities, and instead ask for the next-best solution. This makes good use of the experts’ time, since they are only asked for guidance pertinent to promising solutions.

This innovation was developed by Martin Feather and Steven Cornford of Caltech and Tim Menzies of the University of British Columbia for NASA’s Jet Propulsion Laboratory. Further information is contained in a TSP (see page 1).

This software is available for commercial licensing. Please contact Don Hart of the California Institute of Technology at (818) 393-3425. Refer to NPO-30512.

2 The TechSat 21 Autonomous Sciencecraft Experiment

Software has been developed to perform a number of functions essential to autonomous operation in the Autonomous Sciencecraft Experiment (ASE), which is scheduled to be demonstrated aboard a constellation of three spacecraft, denoted TechSat 21, to be launched by the Air Force into orbit around the Earth in January 2006. A prior version of this software was reported in “Software for an Autonomous Constellation of Satellites” (NPO-30355), *NASA Tech Briefs*, Vol. 26, No. 11 (November 2002), page 44.

The software includes the following components:

- Algorithms to analyze image data, generate scientific data products, and detect conditions, features, and events of

potential scientific interest;

- A program that uses component-based computational models of hardware to analyze anomalous situations and to generate novel command sequences, including (when possible) commands to repair components diagnosed as faulty;
- A robust-execution-management component that uses the Spacecraft Command Language (SCL) software to enable event-driven processing and low-level autonomy; and
- The Continuous Activity Scheduling, Planning, Execution, and Replanning (CASPER) program for replanning activities, including downlink sessions, on the basis of scientific observations performed during previous orbit cycles.

This program was written by Robert Sherwood, Russell Knight, Gregg Rabideau, Steve Chien, Daniel Tran, Benjamin Cichy, Rebecca Castaño, Timothy Stough, and Ashley Davies of Caltech for NASA’s Jet Propulsion Laboratory. Further information is contained in a TSP (see page 1).

This software is available for commercial licensing. Please contact Don Hart of the California Institute of Technology at (818) 393-3425. Refer to NPO-30784.

2 Software for Analyzing Laminar-to-Turbulent Flow Transitions

Langley Stability and Transition Analysis Codes (LASTRAC) is a set of engineering software tools developed with the C++ language and modern software technologies for use in analyzing transition from laminar to turbulent flows. LASTRAC is a product of ongoing NASA Langley research projects related to transition flow physics modeling and simulations. It is intended to be a set of easy-to-use engineering tools that can be applied to routine engineering design studies. At the current stage, LASTRAC is capable of performing transition calculations based on linear stability theory (LST) or linear and nonlinear parabolized stability equations (PSE) for a broad range of flow regimes and configurations of interest for the design of low-speed as well as supersonic and hypersonic vehicles. At present, LASTRAC is limited to two-dimensional, axisymmetric, or infinite

swept-wing boundary layers. Options for general three-dimensional boundary layers are currently under development. The LST option makes it possible to perform traditional N -factor transition correlation. Linear and nonlinear PSE are used to track instability wave evolution from small-amplitude till

early transition stage in a high-fidelity manner. It is planned to incorporate modules in LSTRAC that models the receptivity (the process by which perturbations are introduced into laminar boundary-layer flow) and late stage of the transition process. These software modules are intended to enable LAS-

TRAC to perform computations for different stages of laminar-to-turbulent transition in an integrated fashion.

*This program was written by Chau-Lyan Chang of **Langley Research Center**. Further information is contained in a TSP (see page 1).*
LAR-16260



Elastomer Filled With Single-Wall Carbon Nanotubes

Strength and stiffness increase with SWNT content.

Lyndon B. Johnson Space Center, Houston, Texas

Experiments have shown that composites of a silicone elastomer with single-wall carbon nanotubes (SWNTs) are significantly stronger and stiffer than is the unfilled elastomer. The large strengthening and stiffening effect observed in these experiments stands in contrast to the much smaller strengthening effect observed in related prior efforts to reinforce epoxies with SWNTs and to reinforce a variety of polymers with multiple-wall carbon nanotubes (MWNTs). The relative largeness of the effect in the case of the silicone-elastomer/SWNT composites appears to be attributable to (1) a better match between the ductility of the fibers and the elasticity of the matrix and (2) the greater tensile strengths of

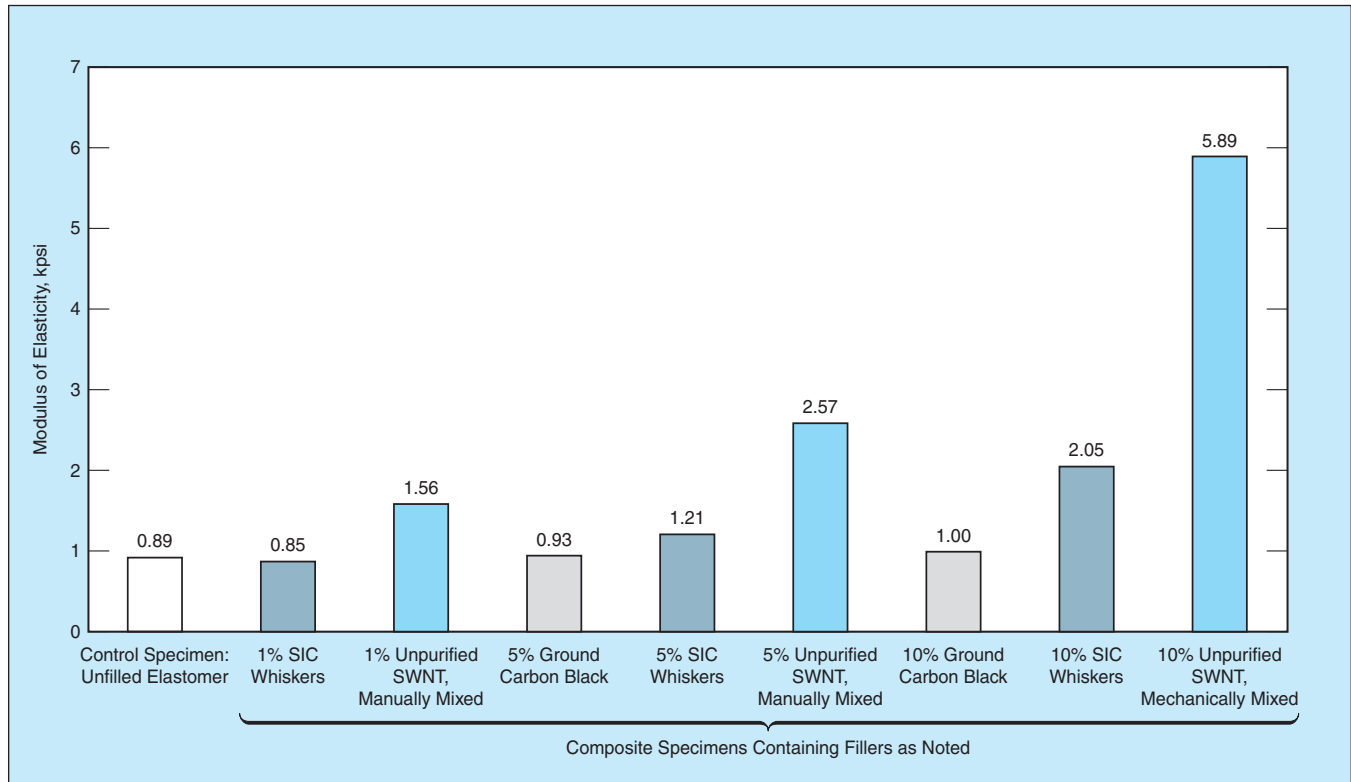
SWNTs, relative to MWNTs.

For the experiments, several composites were formulated by mixing various proportions of SWNTs and other filling materials into uncured RTV-560, which is a silicone adhesive commonly used in aerospace applications. Specimens of a standard "dog-bone" size and shape for tensile testing were made by casting the uncured elastomer/filler mixtures into molds, curing the elastomer, then pressing the specimens from a "cookie-cutter" die.

The results of tensile tests of the specimens showed that small percentages of SWNT filler led to large increases in stiffness and tensile strength, and that these increases were greater than those afforded by other fillers. For example, the

incorporation of SWNTs in a proportion of 1 percent increased the tensile strength by 44 percent and the modulus of elasticity (see figure) by 75 percent. However, the relative magnitudes of the increases decreased with increasing nanotube percentages because more nanotubes made the elastomer/nanotube composites more brittle. At an SWNT content of 10 percent, the tensile strength and modulus of elasticity were 125 percent and 562 percent, respectively, greater than the corresponding values for the unfilled elastomer.

This work was done by Bradley S. Files and Craig R. Forest of Johnson Space Center. Further information is contained in a TSP (see page 1). MSC-23301



The Stiffness of a Silicone Elastomer filled with several different kinds and proportions of reinforcing materials was measured in standard tensile tests.



Modifying Ship Air-Wake Vortices for Aircraft Operations

Takeoffs and landings would be safer.

Langley Research Center, Hampton, Virginia

Columnar-vortex generators (CVG) have been proposed as means to increase the safety of takeoffs and landings of aircraft on aircraft or helicopter carriers and other ships at sea. According to the proposal, CVGs would be installed at critical edge locations on ships to modify the vortices in the air wakes of the ships. The desired effects of modifications are to smooth airflows over takeoff and landing deck areas and divert vortices from takeoff and landing flight paths.

With respect to aircraft operations, the wake flows of primary interest are those associated with the bow and side edges of aircraft-carrier decks and with superstructures of ships in general (see Figure 1). The bow and deck-edge vortices can adversely affect airplane and helicopter operations on carriers, while the superstructure wakes can primarily affect operations of helicopters.

The concept of the CVG is not new; what is new is the proposed addition of CVGs to ship structures to effect favorable modifications of air wakes. Figure 2 depicts a basic CVG, vertical and horizontal CVGs installed on a simple superstructure, and horizontal CVGs installed on the bow and deck edges. The vertical CVGs would be closed at the deck but open at the top. Each horizontal CVG

would be open at both ends. The dimensions of the CVGs installed on the aft edges of the superstructure would be chosen so that the portion of the flow modified by the vertical CVGs would interact synergistically with the portion of the flow modified by the horizontal CVG to move the air wake away from the takeoff-and-landing zone behind the superstructure.

The deck-edge CVGs would be mounted flush with, and would extend slightly ahead of the bow of, the flight deck. The overall length of each tube would exceed that of the flight deck. Each deck-edge CVG would capture that portion of the airflow that generates a deck-edge vortex and would generate a columnar vortex of opposite sense to that of the unmodified vortex. The vortex generated by the CVG could be dispersed at its base, thereby removing unwanted turbulence in the path of an approaching airplane. The deck-edge

CVGs would promote smooth flow over the entire flight deck. In the case of a Nimitz-class aircraft carrier like that of Figure 1, there would be a CVG on each of the outer edges of the two left portions of the flight deck and a single CVG on the right side of the flight deck. The forwardmost CVG on the left side would take the generated vortex underneath the angled flight deck.

A CVG could also be installed on the bow of the flight deck to smooth the flow of air onto the flight deck. In the case of wind incident on the deck from an azimuth other than straight ahead, the vortex generated by the bow CVG could, perhaps, be used to feed the CVG(s) of the leeward side edge of the flight deck.

This work was done by John E. Lamar of Langley Research Center. Further information is contained in a TSP (see page 1). LAR-16281

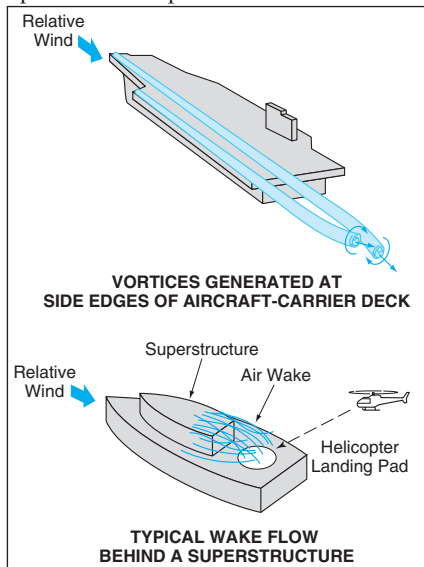


Figure 1. Air Wakes of ship structures can adversely affect operations of aircraft.

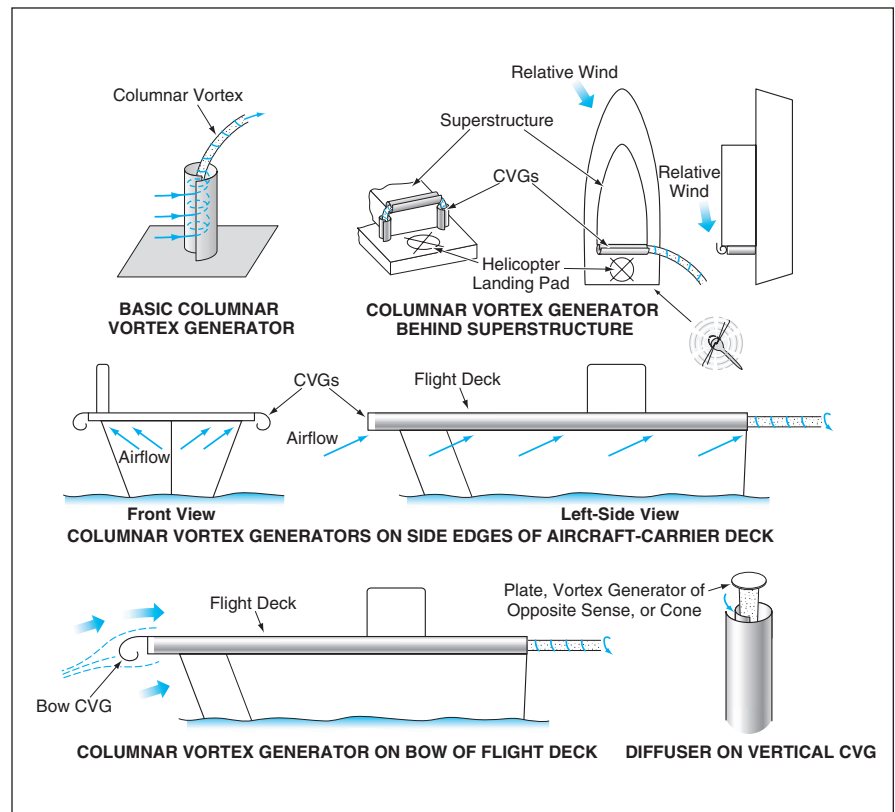


Figure 2. Columnar-Vortex Generators would modify air wakes to provide smoother flows and divert vortices from paths of aircraft.

Strain-Gauge Measurement of Weight of Fluid in a Tank

This method is nonintrusive and independent of the nature of the fluid.

Stennis Space Center, Mississippi

A method of determining the amount of fluid in a tank is based on measurement of strains induced in tank supports by the weight of the fluid. Unlike most prior methods, this method is nonintrusive: there is no need to insert instrumentation in the tank and, hence, no need to run wires, cables, or tubes through the tank wall. Also unlike most prior methods, this method is applicable even if the fluid in the tank is at supercritical pressure and temperature, because it does not depend on the presence of a liquid/gas interface (as in liquid-level-measuring methods).

The strain gauges used in this method may be of two types: foil and fiber-optic. Four foil gauges (full bridge) are mounted on each of the tank-supporting legs. As the tank is filled or emptied, the deformation in each leg increases or decreases, respectively. Measured deformations of all legs are added to obtain a composite deformation indicative of the change in weight of the tank plus fluid. An initial calibration is performed by recording data at two points (usually, empty and full) for which the mass or weight of fluid is known. It is assumed that the deformations are elastic, so that the line passing through the two points can be used as a calibration curve of mass (or weight) of fluid versus deformation.

One or more fiber-optic gauges may be used instead of the foil gauges. The resolution of the fiber-optic and foil gauges is approximately the same, but the fiber-optic gauges are immune to EMI (electromagnetic interference), are linear with respect to temperature over their entire dynamic range (as defined by the behavior of the sample), and mea-

sure thermally induced deformations as predictable signals. Conversely, long term testing has demonstrated that the foil gauges exhibit an erratic behavior whenever subjected to direct sun radiation (even if protected with a rubberized cover). Henceforth, for deployment in outdoor conditions, fiber-optic gauges are the only option if one is to rely on the system for an extended period of time when a recalibration procedure may not be acceptable.

A set of foil gauges had been tested on the supports of a 500-gallon (1,900-liter) tank. The gauges were found to be capable of measuring the deformations (up to 22 micro-strain) that occurred during filling and emptying of the tank. The fluid masses calculated from the gauge readings were found to be accurate within 4.5 percent. However, the reliability of the foil gauges over a few hours was not acceptable. Therefore, the foil sensor system is acceptable for use only in controlled environments (complete shade, or indoors).

The fiber-optic sensors are reliable and at least as accurate as the foil sensors (possibly more). The fiber-optic system consists of one or more sensors mounted on the structure, a temperature sensor also mounted on the structure, and a reference fiber-optic sensor mounted on a plate made of the same material as the tank-supporting legs, that is not subjected to any mechanical load. An important element to consider is the thermal deformation of the structure, which is not going to be exactly the same as that of the reference plate. This is because the structure has appendages (pipes, etc.) that must be taken into account for temperature compensation.

The procedure to calculate a compensated measurement (a measurement reflecting the mass contents of the tank) using the fiber-optic system is as follows: First, one must characterize the structure as it deforms due solely to thermal effects by taking measurements over its operating temperature range, when the tank is empty. During this characterization procedure, deformation and temperature measurements are taken from the sensors attached to the structure (strain and temperature) and the sensor attached to the reference plate (strain). With this information, a tabulated or graphical tool is developed such that at any given temperature, the reference signal is subtracted from the structural signal, and further modified by a value that depends on the structure's temperature. Note that the characterization of the structure as it deforms due to temperature variations may also be done by analytical methods that can model the process. In that case, the experimental characterization is not needed.

It may be possible to increase accuracy further by increasing the signal-to-noise ratio through the use of more deformable tank-supporting legs, larger gauges that measure larger deformations, or other methods to increase the strain in some part of the tank support structure.

This work was done by Jorge Figueroa, William St. Cyr, and Shamim Rahman of Stennis Space Center and Gregory McVay, David Van Dyke, William Mitchell, and Lester Langford of Lockheed Martin Corp.

Inquiries concerning rights for the commercial use of this invention should be addressed to the Intellectual Property Manager, Stennis Space Center, (228) 688-1929. Refer to SSC-00187.

Advanced Docking System With Magnetic Initial Capture

Speeds of approach, and thus docking forces, could be relatively small.

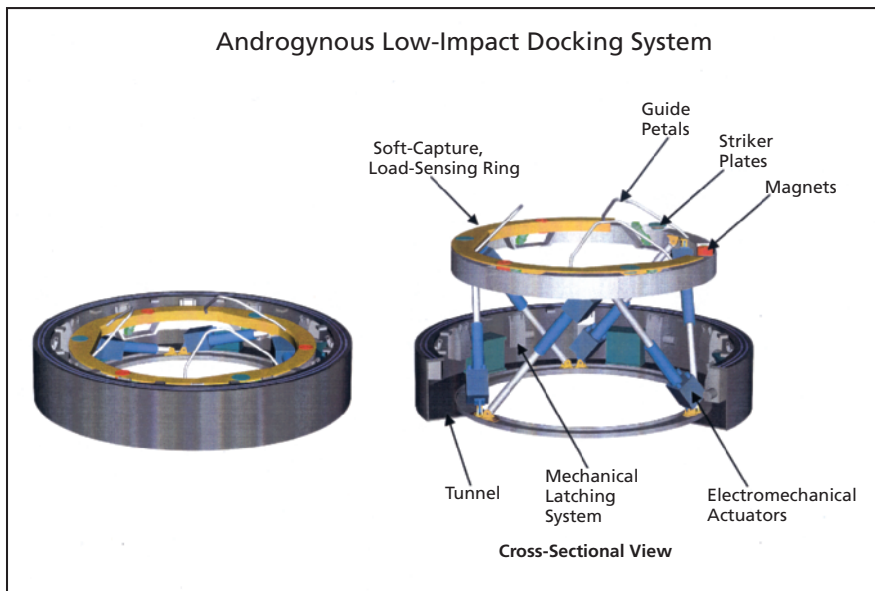
Lyndon B. Johnson Space Center, Houston, Texas

An advanced docking system is undergoing development to enable softer, safer docking than was possible when using prior docking systems. This system is intended for original use in docking of visiting spacecraft and berthing the Crew Re-

turn Vehicle at the International Space Station (ISS). The system could also be adapted to a variety of other uses in outer space and on Earth, including mating submersible vehicles, assembling structures, and robotic berthing/handling of pay-

loads and cargo.

Heretofore, two large spacecraft have been docked by causing the spacecraft to approach each other at a speed sufficient to activate capture latches — a procedure that results in large docking



This Graphical Representation Depicts a Demonstration Version of the advanced docking system for use in berthing an X-38 spacecraft at the International Space Station.

loads and is made more difficult because of the speed. The basic design and mode of operation of the present advanced docking system would eliminate the need to rely on speed of approach to activate capture latches, thereby making it possible to reduce approach speed and thus docking loads substantially.

The system would comprise an active subsystem on one spacecraft and a passive subsystem on another spacecraft with which the active subsystem will be docked. The passive subsystem would include an extensible ring containing magnetic striker plates and guide petals. The active subsystem would include mating guide petals and electromagnets containing limit switches and would be

arranged to mate with the magnetic striker plates and guide petals of the passive assembly. The electromagnets would be carried on (but not rigidly attached to) a structural ring that would be instrumented with load sensors. The outputs of the sensors would be sent, along with position information, as feedback to an electronic control subsystem. The system would also include electro-mechanical actuators that would extend or retract the ring upon command by the control subsystem.

In preparation for docking, one spacecraft would move to a position near (but not touching) the other spacecraft, with the docking ports of the two spacecraft in approximate alignment. Then while one

spacecraft maintained an approximately constant position relative to the other spacecraft, the actuators of the active subsystem would be made to extend the ring, gently pushing the guide petals and electromagnets toward the passive ring guide petals and magnetic striker plates: in effect, the active subsystem would reach out, comply, and grab the passive subsystem.

During this reaching out, the hardware and software of the feedback control subsystem would command the actuators to respond to sensed loads to correct for any misalignments between the docking ports, i.e., to comply. The reaching-out-and-alignment process would continue until the limit switches indicated soft capture — i.e., final petal alignment and magnetic capture of the magnetic striker plates. Once soft capture and alignment was complete, the ring would be retracted, then mechanical latches would be engaged to secure the docked spacecraft to each other.

The active subsystem ring, electromagnets, and petals would then be withdrawn, and the latches would continue to hold the spacecraft together. Later, the undocking could be effected by releasing the mechanical latches.

This work was done by James L. Lewis of Johnson Space Center and Monty B. Carroll, Ray Morales, and Thang Le of Lockheed Martin.

This invention has been patented by NASA (U.S. Patent No. 6,354,540). Inquiries concerning nonexclusive or exclusive license for its commercial development should be addressed to the Patent Counsel, Johnson Space Center, (281) 483-0837. Refer to MSC-22931.



Blade-Pitch Control for Quieting Tilt-Rotor Aircraft

Actively induced harmonic blade-pitch oscillations reduce BVI noise.

Ames Research Center, Moffett Field, California

A method of reducing the noise generated by a tilt-rotor aircraft during descent involves active control of the blade pitch of the rotors. This method is related to prior such noise-reduction methods, of a type denoted generally as higher-harmonic control (HHC), in which the blade pitch is made to oscillate at a harmonic of the frequency of rotation of the rotor.

A tilt-rotor aircraft is so named because mounted at its wing tips are motors that can be pivoted to enable the aircraft to take off and land like a helicopter or to fly like a propeller airplane. When the aircraft is operating in its helicopter mode, the rotors generate more thrust per unit rotor-disk area than helicopter rotors do, thus producing more blade-vortex interaction (BVI) noise. BVI is a major source of noise produced by helicopters and tilt-rotor aircraft during descent: When a rotor descends into its own wake, the interaction of each blade with the blade-tip vortices generated previously gives rise to large air-pressure fluctuations. These pressure fluctuations radiate as distinct, impulsive noise.

In general, the pitch angle of the rotor blades of a tilt-rotor aircraft is controlled by use of a wash plate connected to the rotor blades by pitch links. In both prior HHC methods and the present method, HHC control signals are fed as input to wash-plate control actuators, causing the rotor-blade pitch to oscillate. The amplitude, frequency, and phase of the control signal can be chosen to minimize BVI noise.

In the present method, one typically chooses a control waveform that causes the blade pitch to oscillate sinusoidally at the $N+1$ harmonic of the rotation frequency (where N is the number of blades on each rotor). The phase of the oscillation is typically chosen such that the minimum pitch angle occurs at a fixed rotor-blade azimuth angle within the range from 60° to 90° (where 0° azimuth is defined as directly aft). The phase is critical, but the amplitude is not: It has been found that pitch-angle oscillation amplitudes up to approximately 0.7° can result in large reductions of noise. Larger pitch amplitudes

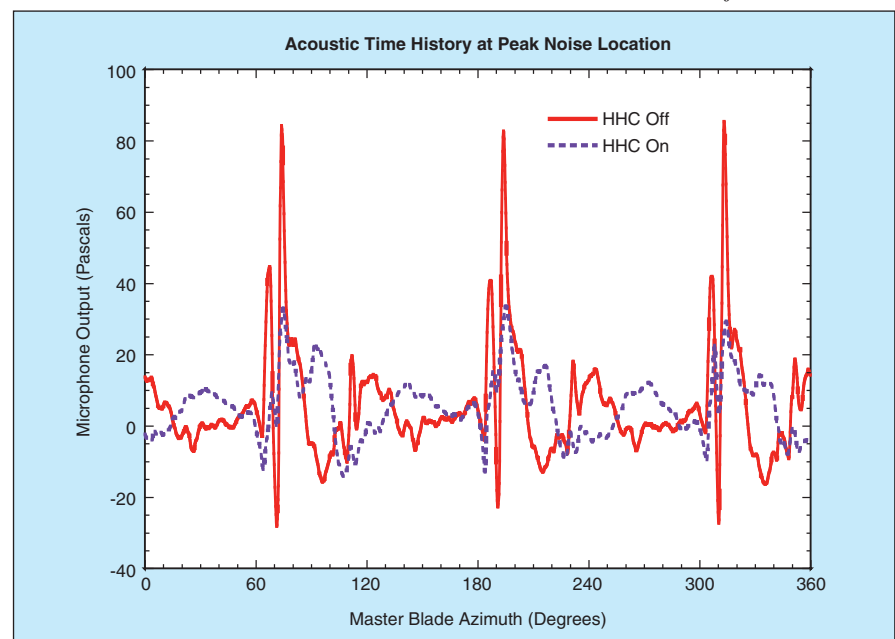
can result in larger reductions of noise, but one might prefer to avoid them because they are accompanied by increases in control loads.

Prior efforts to exploit the HHC concept to reduce helicopter vibration and noise have been oriented toward the development of complex, closed-loop control systems that would utilize feedback from sensors and that would implement iterative control algorithms to adjust HHC settings to optimize responses over the full ranges of operating conditions. The development of such systems can be expensive and time-consuming. In contrast, a system according to the present method is relatively simple because it is an open-loop system. By selecting a single harmonic (the $N+1$) and fixing the amplitude, one can reduce the problem of choosing the control signal to one of selecting a single open-loop input signal (the phase signal), which can be optimized for several descending flight conditions. In other words, HHC phase values can be predetermined and scheduled for specific flight conditions. The schedule of phase values can be implemented by use of control software and hardware.

The pilot can turn the HHC system on or off by means of a switch (see figure). Ordinarily, the HHC system would be used only when reduction of noise was desired during descent in the helicopter mode. Because the time spent in use of the HHC system would ordinarily be a small fraction of the total operational time of the aircraft, the control loads associated with use of the HHC system could be expected to cause little, if any reduction, in the lifetime of the mechanical components of the pitch-control system. Because the HHC noise-reduction system is not needed for safe operation of the aircraft, it is a fail-safe system: The system can be switched off at any time without adversely affecting flight, the only penalty being an increase in noise.

This work was done by Mark D. Betzina and Khanh Q. Nguyen of Ames Research Center. Further information is contained in a TSP (see page 1).

This invention is owned by NASA, and a patent application has been filed. Inquiries concerning nonexclusive or exclusive license for its commercial development should be addressed to the Patent Counsel, Ames Research Center, (650) 604-5104. Refer to ARC-14606.



This Graph Demonstrates the Effect of HHC on acoustic time history at peak directivity.

⚙️ Solar Array Panels With Dust-Removal Capability

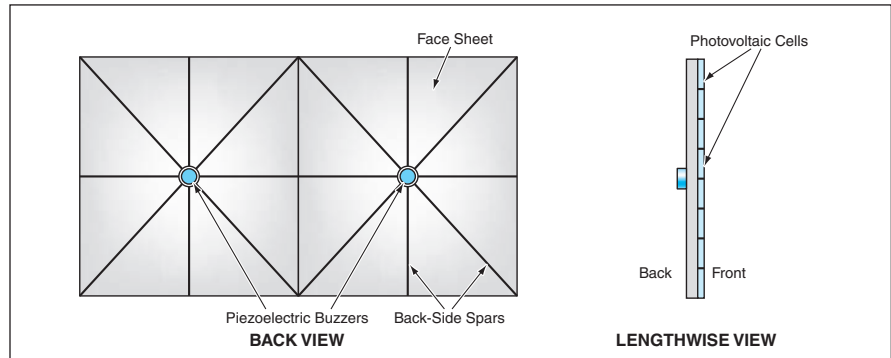
Inexpensive, low-power piezoelectric buzzers would be built in.

NASA's Jet Propulsion Laboratory, Pasadena, California

It has been proposed to incorporate piezoelectric vibrational actuators into the structural supports of solar photovoltaic panels, for the purpose of occasionally inducing vibrations in the panels in order to loosen accumulated dust. Provided that the panels were tilted, the loosened dust would slide off under its own weight. Originally aimed at preventing obscuration of photovoltaic cells by dust accumulating in the Martian environment, the proposal may also offer an option for the design of solar photovoltaic panels for unattended operation at remote locations on Earth.

The figure depicts a typical lightweight solar photovoltaic panel comprising a backside grid of structural spars that support a thin face sheet that, in turn, supports an array of photovoltaic cells on the front side. The backside structure includes node points where several spars intersect. According to the proposal, piezoelectric buzzers would be attached to the node points. The process of designing the panel would be an iterative one that would include computational simulation of the vibrations by use of finite-element analysis to guide the selection of the vibrational frequency of the actuators and the cross sections of the spars to maximize the agitation of dust.

Although the basic concept of the proposal is a straightforward extension of a common household cleaning practice, the engineering implementation of the proposal would not be trivial. The following are some of the engineering issues that must be addressed:



Piezoelectric Buzzers would be mounted at nodes of a grid of spars that support a solar photovoltaic panel.

- Compact, low-power, inexpensive piezoelectric buzzers are commercially available. They may or may not be suitable for use as the piezoelectric actuators to implement the proposal. Because typical commercial buzzers operate in the kilohertz frequency range and the natural vibrational frequencies of typical solar photovoltaic panels are lower, it may be necessary to build lower-frequency piezoelectric buzzers.
- It may be necessary to cover panels with flat, transparent sheets or else redesign the panels to eliminate recesses or protrusions that could retain dust or prevent dust from sliding off during vibration.
- The expected rate of accumulation of dust must be taken into account in assessing the effectiveness of a dust-removal design.
- Tests must be performed to determine the interdependences among tilt angles required for interception of solar radiation, the amounts of agitation re-

quired at various vibrational frequencies and amplitudes to reduce obscuration by dust to an acceptably low level at those tilt angles, and the differences in among the rates of removal of dust particles of different sizes and types.

- Care must be taken to ensure that the energy recovered by removing dust that obscures the solar photovoltaic panel exceeds the energy expended in shaking the dust off. This entails consideration of buzzer power levels and agitation times.
- Care must also be taken to ensure that the dust-removal design does not adversely affect equipment other than the solar photovoltaic panel.

This work was done by Stephen Dawson, Nick Mardesich, Brian Spence, and Steve White of Caltech for NASA's Jet Propulsion Laboratory. Further information is contained in a TSP (see page 1). NPO-30909

Aligning Arrays of Lenses and Single-Mode Optical Fibers

A procedure for precise alignment involves the use of an interferometer and positioning stages.

NASA's Jet Propulsion Laboratory, Pasadena, California

A procedure now under development is intended to enable the precise alignment of sheet arrays of microscopic lenses with the end faces of a coherent bundle of as many as 1,000 single-mode optical fibers packed closely in a regular array (see Figure 1). In the original application that prompted this development, the precise assembly of lenses and optical fibers serves as a single-mode spatial filter for a visible-light nulling interferometer. The precision of alignment must be sufficient to limit any remaining wavefront error to a root-mean-square

value of less than 1/10 of a wavelength of light. This wavefront-error limit translates to requirements to (1) ensure uniformity of both the lens and fiber arrays, (2) ensure that the lateral distance from the central axis of each lens and the corresponding optical fiber is no more than a fraction of a micron, (3) angularly align the lens-sheet planes and the fiber-bundle end faces to within a few arc seconds, and (4) axially align the lenses and the fiber-bundle end faces to within tens of microns of the focal distance.

Figure 2 depicts the apparatus used in

the alignment procedure. The beam of light from a Zygo (or equivalent) interferometer is first compressed by a ratio of 20:1 so that upon its return to the interferometer, the beam will be magnified enough to enable measurement of wavefront quality. The apparatus includes relay lenses that enable imaging of the arrays of microscopic lenses in a charge-coupled-device (CCD) camera that is part of the interferometer. One of the arrays of microscopic lenses is mounted on a 6-axis stage, in proximity to the front face of the bundle of optical fibers. The bundle is mounted on a separate stage. A mirror is attached to the back face of the bundle of optical fibers for retroreflection of light. When a microscopic lens and a fiber are aligned with each other, the affected portion of the light is reflected back by the mirror, recollimated by the microscopic lens, transmitted through the relay lenses and the beam compressor/expander, then split so that half goes to a detector and half to the interferometer. The output of the detector is used as a feedback control signal for the six-axis stage to effect alignment.

The alignment procedure, which is rather complex, can be summarized as follows:

1. In the absence of a sheet array of microscopic lenses, the longitudinal axis

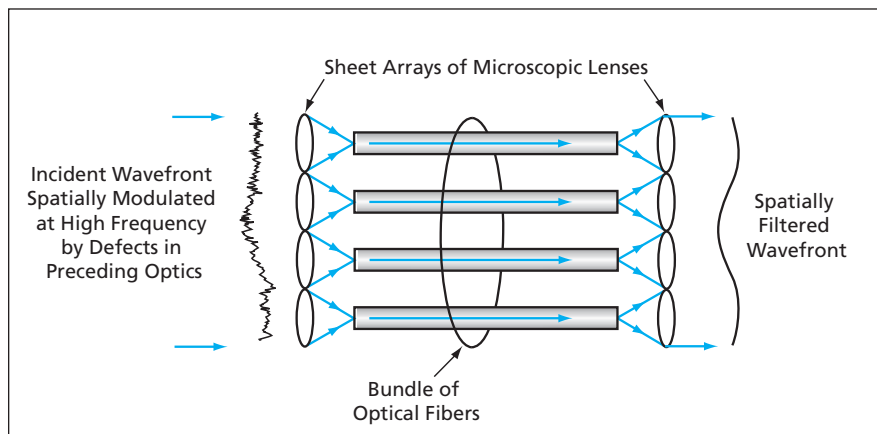


Figure 1. The **Problem Is To Align** two sheet arrays of microscopic lenses with polished end faces of a bundle of optical fibers. The assembly of lenses and fibers is meant to act as a spatial filter.

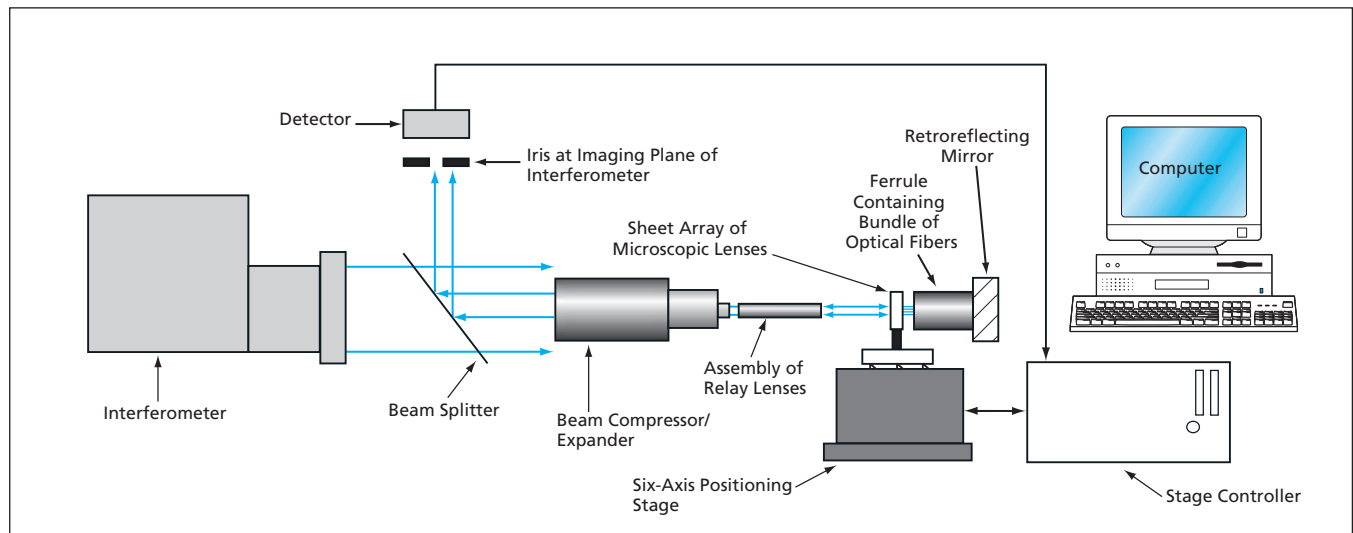


Figure 2. An **Interferometer** is used along with a six-axis positioning stage (and other positioning stages omitted from this view for clarity) to measure and correct the relative position and orientation of the bundle of optical fibers and the sheet array of microscopic lenses.

- of the fiber-optic bundle is aligned with the optical axis of the interferometer by use of the reflection from the front face of the bundle.
2. One of the sheet arrays of microscopic lenses is placed in front of the fiber-optic bundle and similarly aligned with the interferometer optical axis by use of the reflection from its front face. As a result, the optical axes of the lens array and the fiber-optic bundle are parallel with each other.
 3. The axial position of the lens sheet is adjusted until the interferometric image of light reflected from the front face of the fiber-optic bundle indicates that the lenses are at the proper focal distance.
 4. The lateral (relative to the optical axis) position of the lens sheet is adjusted until the interferometric image shows that at least one lens is

- centered on the end of at least one optical fiber. The lateral coordinates of the six-axis positioner are measured. The lateral position of the lens sheet is further adjusted until another lens/fiber pair is thus centered, and the corresponding coordinates are measured. The two sets of coordinates are used to compute the translation and rotation needed to effect the lateral alignment of the remaining lens/fiber pairs.
5. Guided by the foregoing coordinate measurements, the final adjustments of the lens sheet are made.
 6. The lens sheet is bonded to the fiber-optic bundle.
 7. The fiber-optic bundle is turned around so that what was previously the back face is now the front face.
 8. The retroreflecting mirror is aligned with the optical axis of the interferometer.

9. Steps 1 through 7 are repeated to effect the alignment and bonding of the second lens sheet to what is now the front face of the fiber-optic bundle.

This work was done by Duncan Liu of Caltech for NASA's Jet Propulsion Laboratory. Further information is contained in a TSP (see page 1).

In accordance with Public Law 96-517, the contractor has elected to retain title to this invention. Inquiries concerning rights for its commercial use should be addressed to:

*Innovative Technology Assets Management
JPL*

Mail Stop 202-233

4800 Oak Grove Drive

Pasadena, CA 91109-8099

(818) 354-2240

E-mail: iaoffice@jpl.nasa.gov

Refer to NPO-40021, volume and number of this NASA Tech Briefs issue, and the page number.

Automatic Control of Arc Process for Making Carbon Nanotubes

Lyndon B. Johnson Space Center, Houston, Texas

An automatic-control system has been devised for a process in which carbon nanotubes are produced in an arc between a catalyst-filled carbon anode and a graphite cathode. The control system includes a motor-driven screw that adjusts the distance between the electrodes. The system also includes a bridge circuit that puts out a voltage proportional to the difference between (1) the actual value of potential drop across the arc and (2) a reference value

between 38 and 40 V (corresponding to a current of about 100 A) at which the yield of carbon nanotubes is maximized. Utilizing the fact that the potential drop across the arc increases with the inter-electrode gap, the output of the bridge circuit is fed to a motor-control circuit that causes the motor to move the anode toward or away from the cathode if the actual potential drop is more or less, respectively, than the reference potential. Thus, the system regulates the

interelectrode gap to maintain the optimum potential drop. The system also includes circuitry that records the potential drop across the arc and the relative position of the anode holder as function of time.

*This work was done by Carl D. Scott of Johnson Space Center, Robert B. Pulumbarit of Lockheed Martin, and Joe Victor of Hernandez Engineering. Further information is contained in a TSP (see page 1).
MSC-23134*

Curved-Focal-Plane Arrays Using Deformed-Membrane Photodetectors

It would not be necessary to perform fabrication processing of curved substrates.

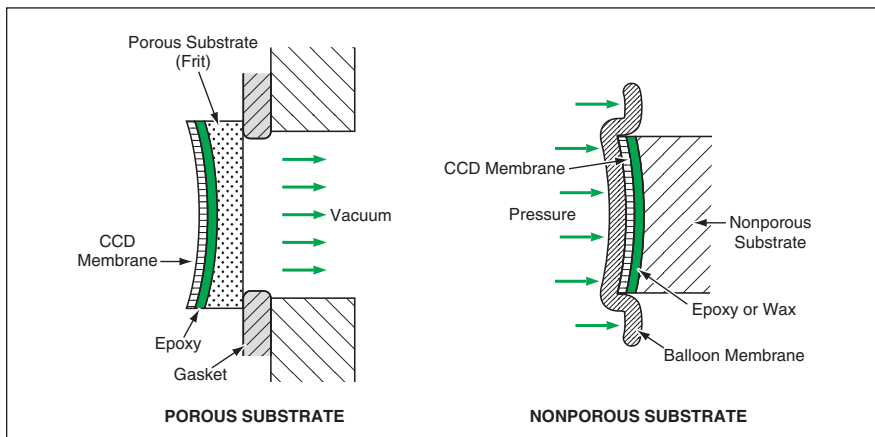
NASA's Jet Propulsion Laboratory, Pasadena, California

A versatile and simple approach to the design and fabrication of curved-focal-plane arrays of silicon-based photodetectors is being developed. This approach is an alternative to the one described in "Curved Focal-Plane Arrays Using Back-Illuminated High-Purity Photodetectors" (NPO-30566), *NASA Tech Briefs*, Vol. 27, No. 10 (October 2003), page 10a.

As in the cited prior article, the basic idea is to improve the performance of an imaging instrument and simplify the optics needed to obtain a given level of performance by making an image sensor (in this case, an array of photodetectors) conform to a curved focal surface, instead of designing the optics to project an image onto a flat focal surface. There

is biological precedent for curved-focal-surface designs: retinas — the image sensors in eyes — conform to the naturally curved focal surfaces of eye lenses.

The present approach is applicable to both front-side- and back-side-illuminated, membrane photodetector arrays and is being demonstrated on charge-coupled devices (CCDs). The very-large-



A Flat Membrane CCD would be pressed against, and bonded to, a curved substrate in either of two ways.

scale integrated (VLSI) circuitry of such a CCD or other array is fabricated on the front side of a silicon substrate, then the CCD substrate is attached temporarily to a second substrate for mechanical support, then material is removed from the back to obtain the CCD membrane, which typically has a thickness between 10 and 20 μm . In the case of a CCD designed to operate in back-surface illumination, delta doping can be performed after thinning to enhance the sensitivity. This approach is independent of the design and method of fabrication of the front-side VLSI circuitry and does not involve any processing of a curved silicon substrate.

In this approach, a third substrate would be prepared by polishing one of its surfaces to a required focal-surface curvature. A CCD membrane fabricated as described above would be pressed against, deformed into conformity with, and bonded to, the curved surface. The technique used to press and bond the CCD membrane would depend on the nature of the supporting material (see figure). For example, if the third substrate were made of quartz frit, the substrate would be prepared by suffusing it with epoxy. Then one would take advantage of the porosity of the frit by applying a partial vacuum to the opposite sur-

face of the frit, causing atmospheric pressure to push the CCD membrane against the curved surface. The curing of the epoxy would bond the CCD membrane to the curved surface.

Alternatively, if the third substrate were made of a nonporous material, the curved substrate surface would be prepared by coating it with a wax or an uncured epoxy. The CCD membrane would be pressed against the coated, curved surface by use of a suitably pressurized balloon. The CCD membrane would then become bonded to the curved surface by curing of the epoxy or freezing of the wax.

This work was done by Shouleh Nikzad and Todd Jones of Caltech for NASA's Jet Propulsion Laboratory. Further information is contained in a TSP (see page 1).

In accordance with Public Law 96-517, the contractor has elected to retain title to this invention. Inquiries concerning rights for its commercial use should be addressed to

Intellectual Assets Office

JPL

Mail Stop 202-233

4800 Oak Grove Drive

Pasadena, CA 91109

(818) 354-2240

E-mail: ipgroup@jpl.nasa.gov

Refer to NPO-30580, volume and number of this NASA Tech Briefs issue, and the page number.



Role of Meteorology in Flights of a Solar-Powered Airplane

Meteorological support helped ensure safety and success of experimental high-altitude flights.

Dryden Flight Research Center, Edwards, California

In the summer of 2001, the Helios prototype solar-powered uninhabited aerial vehicle (UAV) [a lightweight, remotely piloted airplane] was deployed to the Pacific Missile Range Facility (PMRF), at Kauai, Hawaii, in an attempt to fly to altitudes above 100,000 ft (30.48 km). The goal of flying a UAV to such high altitudes has been designated a level-I milestone of the NASA Environmental Research Aircraft and Sensor Technology (ERAST) program. In support of this goal, meteorologists from NASA Dryden Flight Research Center were sent to PMRF, as part of the flight crew, to provide current and forecast weather information to the pilots, mission directors, and planners. Information of this kind is needed to optimize flight conditions for peak aircraft performance and to enable avoidance of weather conditions that could adversely affect safety.

In general, the primary weather data of concern for ground and flight operations are wind speeds (see Figure 1). Because of its long wing span [247 ft (≈ 75 m)] and low weight [1,500 to 1,600 lb (about 680 to 726 kg)], the Helios airplane is sensitive to wind speeds exceeding 7 kn (3.6 m/s) at the surface. Also, clouds are of concern because they can block sunlight needed to energize an array of solar photovoltaic cells that provide power to the airplane. Vertical wind shear is very closely monitored in order to prevent damage or loss of control due to turbulence.

Two flights were successfully completed during the deployment at PMRF (see Figure 2). The sequence of meteorological activities in support of each flight included the following:

- Daily forecasts of surface and upper-level meteorological conditions were issued, 48 hours before the planned flight day.
- Current and forecast weather conditions were described at briefings of the crew.
- A weather briefing was given in early morning on the planned flight day to help determine whether the airplane should be taken out of its hangar and prepared for flight.

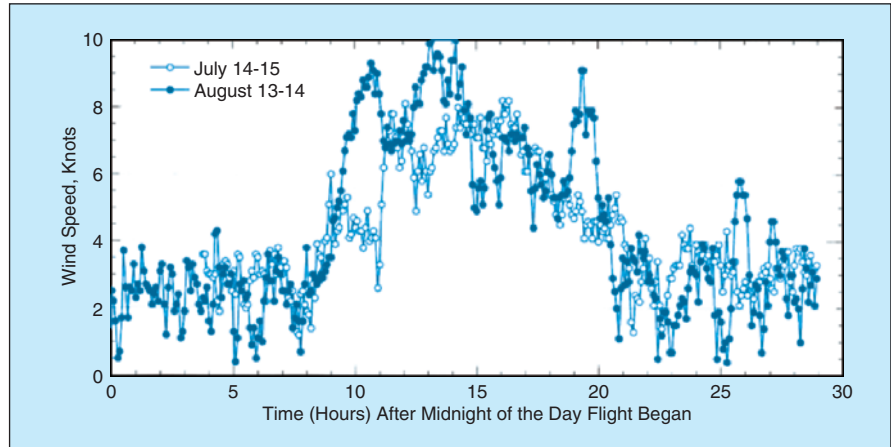
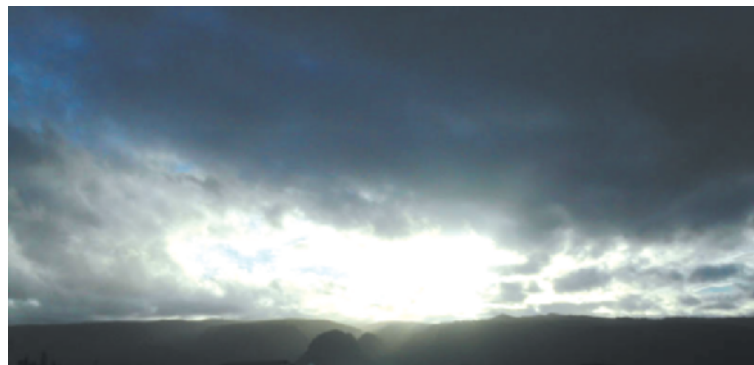


Figure 1. These **Surface-Wind Histories** were recorded at PMRF during intervals that included two flights. Data like these, plus other data, are needed to increase the likelihood of safe and successful flight.



Clouds as Seen From Runway After Sunrise



Helios Prototype Airplane at Takeoff on its Way to a Record Altitude on August 13, 2001

Figure 2. The **Takeoff of the Helios Prototype Solar-Powered UAV** was delayed because of clouds. The airplane then took off and flew to a record altitude.

- A final such “go/no-go” briefing was given 2 hours prior to scheduled take-off.
- After takeoff, periodic updates based of weather-balloon and satellite data were provided to the pilot and mission planner.
- Approximately 2 hours before landing, a final weather forecast was issued to enable estimation of the earliest possible landing time and selection of a runway.
- After landing, surface conditions were monitored until the airplane was safely in the hangar.

The first successful flight took place on July 14, 2001. The takeoff was delayed for 20 minutes because of clouds. Convection over the runway generated moderate turbulence during takeoff. The airplane climbed to a maximum altitude of 76,500 ft (≈ 23.3 km). The airplane landed in stable conditions after more than 15 hours of flight.

The second successful flight took place on August 13, 2001. This time, the takeoff was delayed 45 minutes because of clouds. Strong wind shear due to strong trade winds and island wake was observed at an altitude of 2,000 ft (≈ 600

m). The airplane then climbed until it reached a world-record altitude for a non-rocket-powered aircraft — 96,863 ft (29,524 m). This altitude is more than 11,000 ft (≈ 3.35 km) higher than the record set in a flight of the SR-71 airplane. The airplane landed safely after a last-minute change in runway because of winds.

This work was done by Casey Donohue of AS&M, Inc., for Dryden Flight Research Center. For further information, contact the Dryden Commercial Technology Office at (661) 276-3689. DRC-02-25

Model of Mixing Layer With Multicomponent Evaporating Drops

Effects of multiple chemical components are represented with computational efficiency.

NASA's Jet Propulsion Laboratory, Pasadena, California

A mathematical model of a three-dimensional mixing layer laden with evaporating fuel drops composed of many chemical species has been derived. The study is motivated by the fact that typical real petroleum fuels contain hundreds of chemical species. Previously, for the sake of computational efficiency, spray studies were performed using either models based on a single representative species or models based on surrogate fuels of at most 15 species. The present multicomponent model makes it possible to perform more realistic simulations by accounting for hundreds of chemical species in a computationally ef-

ficient manner.

The model is used to perform Direct Numerical Simulations in continuing studies directed toward understanding the behavior of liquid petroleum fuel sprays. The model includes governing equations formulated in an Eulerian and a Lagrangian reference frame for the gas and the drops, respectively. This representation is consistent with the expected volumetrically small loading of the drops in gas (of the order of 10^{-3}), although the mass loading can be substantial because of the high ratio (of the order of 10^3) between the densities of liquid and gas. The drops are treated as point sources of

mass, momentum, and energy; this representation is consistent with the drop size being smaller than the Kolmogorov scale. Unsteady drag, added-mass effects, Basset history forces, and collisions between the drops are neglected, and the gas is assumed calorically perfect.

The model incorporates the concept of continuous thermodynamics, according to which the chemical composition of a fuel is described probabilistically, by use of a distribution function. Distribution functions generally depend on many parameters. However, for mixtures of homologous species, the distribution can be approximated with acceptable accuracy as a sole function of the molecular weight. The mixing layer is initially laden with drops in its lower stream, and the drops are colder than the gas. Drop evaporation leads to a change in the gas-phase composition, which, like the composition of the drops, is described in a probabilistic manner.

The advantage of the probabilistic description is that while a wide range of individual species can be accommodated in the mixture, the number of governing equations is increased minimally over that necessary for a single species because the composition is represented only by the parameter(s) necessary to construct the distribution function. Here the distribution function is entirely defined by the mean and variance. For this choice of distribution function, the model accounts for evaporation-induced changes in the composition of fuel drops and the surrounding gas, yet involves only two more conservation equations (one for the mean and one for the

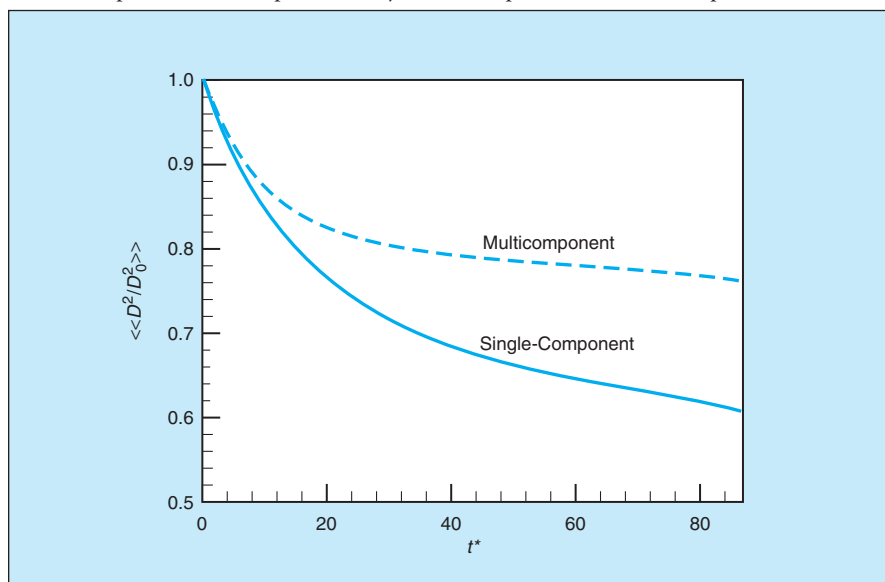


Figure 1. The Evolution of Residual Droplet Areas was computed for the single-component and multicomponent cases. Here t^* is time in units of a characteristic time calculated from initial parameters of the mixing layer, D_0 is the initial drop diameter, D is the drop diameter as a function of time, and $\langle\langle \rangle\rangle$ denotes an ensemble average.

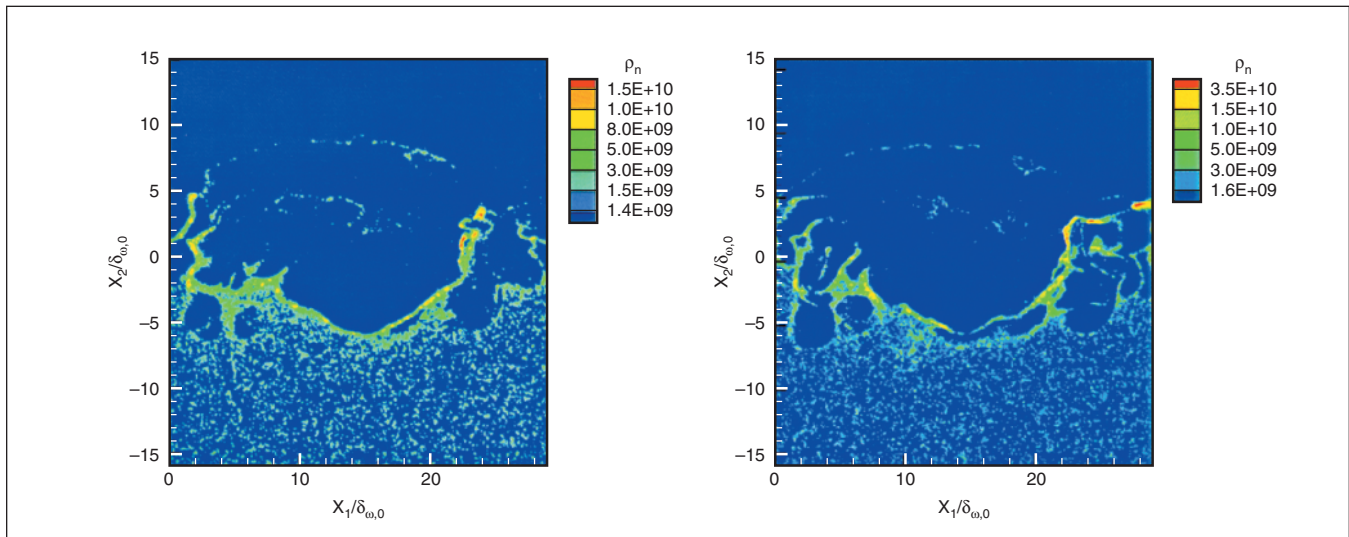


Figure 2. Drop Number Density is shown in a representative plane at the final computation time: (a) single-component drop layer and (b) multicomponent drop layer.

variance) than does an equivalent model for a single-component fuel. The initial mathematical form of the distribution function is postulated to be retained during the drop lifetime, but with evolving mean and variance as the drops evaporate.

In a test, a mixing-layer simulation was performed for drops of single-component-fuel and another such simulation for drops of a multicomponent fuel. Analysis of the results revealed that although the global layer characteristics were similar in the single-component and multicomponent cases, the drops evaporated more slowly in the

multicomponent than in the single-component case (see Figure 1). The slower evaporation of the multicomponent drops was primarily attributed to the lower volatility of higher molar-weight species and to condensation of these species on drops transported in regions of different gas composition. The more volatile species released in the gas phase earlier during the drop lifetime were found to be entrained in the mixing layer, whereas the heavier species that evaporated later during the drop lifetime tended to reside in regions of high drop-number density. This behavior was found to lead to seg-

regation of species in the gas phase on the basis of the relative evaporation time from the drops. The slower evaporation of multicomponent fuel drops was found to lead to regions of higher drop-number density in the drop-laden layer and to permit greater interaction of the drops with the flow, resulting in a more developed small-scale structure (see Figure 2).

This work was done by Josette Bellan and Patrick Le Clercq of Caltech for NASA's Jet Propulsion Laboratory. Further information is contained in a TSP (see page 1). NPO-30505

Solution-Assisted Optical Contacting

Components in optical contact can be adjusted for about a minute.

NASA's Jet Propulsion Laboratory, Pasadena, California

A modified version of a conventional optical-contact procedure has been found to facilitate alignment of optical components. The optical-contact procedure (called simply "optical contacting" in the art) is a standard means of bonding two highly polished and cleaned glass optical components without using epoxies or other adhesives. In its unmodified form, the procedure does not involve the use of any foreign substances at all: components to be optically contacted are dry. The main disadvantage of conventional optical contacting is that it is difficult or impossible to adjust the

alignment of the components once they have become bonded.

In the modified version of the procedure, a drop of an alcohol-based optical cleaning solution (isopropyl alcohol or similar) is placed at the interface between two components immediately before putting the components together. The solution forms a weak bond that gradually strengthens during a time interval of the order of tens of seconds as the alcohol evaporates. While the solution is present, the components can be slid, without loss of contact, to perform fine adjustments of their relative positions.

After about a minute, most of the alcohol has evaporated and the optical components are rigidly attached to each other. If necessary, more solution can be added to enable resumption or repetition of the adjustment until the components are aligned to the required precision.

This work was done by Daniel Shaddock and Alexander Abramovici of Caltech for NASA's Jet Propulsion Laboratory. Further information is contained in a TSP (see page 1). NPO-30731

Improved Discrete Approximation of Laplacian of Gaussian

This method reduces the amount of circuitry needed for filtering of video data.

Lyndon B. Johnson Space Center, Houston, Texas

An improved method of computing a discrete approximation of the Laplacian of a Gaussian convolution of an image has been devised. The primary advantage of the method is that without substantially degrading the accuracy of the end result, it reduces the amount of information that must be processed and thus reduces the amount of circuitry needed to perform the Laplacian-of-Gaussian (LOG) operation.

Some background information is necessary to place the method in context. The method is intended for application to the LOG part of a process of real-time digital filtering of digitized video data that represent brightnesses in pixels in a square array. The particular filtering process of interest is one that converts pixel brightnesses to binary form, thereby reducing the amount of information that must be performed in subsequent correlation processing (e.g., correlations between images in a stereoscopic pair for determining distances or correlations between successive frames of the same image for detecting motions). The Laplacian is often included in the filtering process because it emphasizes edges and textures, while the Gaussian is often included because it smooths out noise that might not be consistent between left and right images

or between successive frames of the same image.

For the purpose of processing digitized image data, the Gaussian and Laplacian values of a pixel of interest are approximated as weighted sums of brightnesses of the pixels in a square subarray (typically 3×3) of pixels centered on the pixel of interest. The weights are represented by coefficient matrices, the elements of which correspond to pixels in the subarray. For example,

$$\begin{pmatrix} 0 & -1 & 0 \\ -1 & 4 & -1 \\ 0 & -1 & 0 \end{pmatrix}$$

gives a reasonable approximation of the Laplacian for a 3×3 subarray.

A typical prior state-of-the-art LOG algorithm operates in a sequential raster-oriented pixel stream, and the kernel is factored as much as possible into 1×3 and 3×1 components. To apply a 1×3 or a 3×1 kernel to the pixel in a given row and column, it is necessary to retain the pixel stream in two raster-length delay lines so that the pixels in the adjacent rows and columns remain available for the computation. Heretofore, 12 bits of precision have been needed to maintain accuracy sufficient for reasonable convolution re-

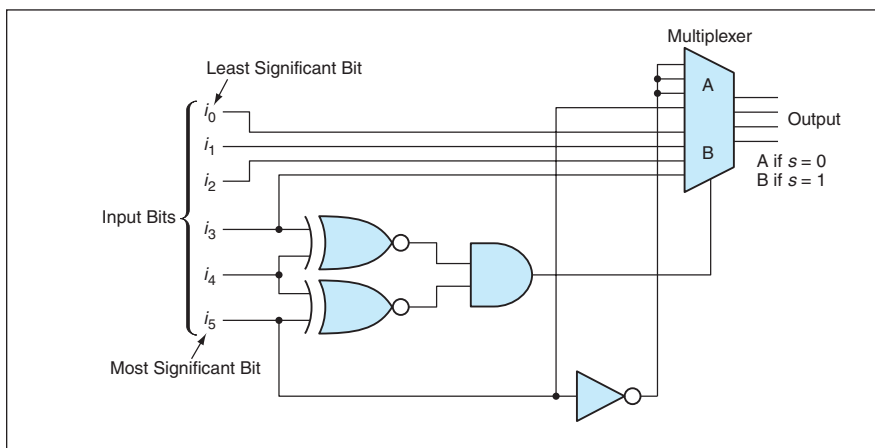
sults through several stages. Usually, the Laplacian operation is performed first to normalize the image data about 0. This concludes the background information.

In the present method, intermediate results are approximated in such a way that only 6 or possibly even as few as four bits are retained, yet the final result is still reasonable. If only 6 bits of precision are needed rather than 12, the size of the memory circuitry needed to implement the delay lines can be halved. Thus, it should be possible to build smaller, lower-power filtering circuits.

Heretofore, it has been common practice in limited-precision arithmetic circuitry to approximate large values by truncating them, eliminating the least significant bits. However, a detailed analysis of the arithmetic process shows that eliminating the bits of lowest order can lead to errors in the final conversion to binary representation. In the present method, the least significant bits are retained and large values are approximated by a saturation technique based on the unconventional approach of discarding the highest-order bits. If the magnitude of a pixel value is larger than the largest magnitude that can be represented in the result, then the pixel value is replaced by a value of the same sign (positive or negative) and the largest representable magnitude.

The figure depicts an example of a circuit that utilizes 2's-complement encoding of negative numbers and that implements saturation of a six-bit quantity to a four-bit quantity. The exclusive-OR gates examine the number of high-order bits to be eliminated, plus one, to determine whether they are already all alike. If the examined input bits are not all alike, a maximum positive or negative quantity is derived from the sign bit and gated through the multiplexer. This is easily extended to handle a reduction of any number of bits.

This work was done by Robert L. Shuler, Jr., of Johnson Space Center. Further information is contained in a TSP (see page 1). MSC-22954



The Input Bits Are Passed through to the multiplexer as long as the magnitude of the input quantity does not exceed a preset four-bit saturation value; if it does exceed that value, then the output has the saturation magnitude and the same sign as that of the input.

Utilizing Expert Knowledge in Estimating Future STS Costs

John F. Kennedy Space Center, Florida

A method of estimating the costs of future space transportation systems (STSs) involves classical activity-based cost (ABC) modeling combined with systematic utilization of the knowledge and opinions of experts to extend the process-flow knowledge of existing systems to systems that involve new materials and/or new architectures. The expert knowledge is particularly helpful in filling gaps that arise in computational models of processes because of inconsistencies in historical cost data. Heretofore, the costs of planned STSs have been estimated following a “top-down” approach that tends

to force the architectures of new systems to incorporate process flows like those of the space shuttles. In this ABC-based method, one makes assumptions about the processes, but otherwise follows a “bottoms up” approach that does not force the new system architecture to incorporate a space-shuttle-like process flow. Prototype software has been developed to implement this method. Through further development of software, it should be possible to extend the method beyond the space program to almost any setting in which there is a need to estimate the costs of a new system and

to extend the applicable knowledge base in order to make the estimate.

*This work was done by David B. Fortner of Command and Control Technologies, Inc., and Alex J. Ruiz-Torres of the University of Texas at El Paso for **Kennedy Space Center**. For further information, contact*

Kevin Brown

Command and Control Technologies

1425 Chaffee Drive, Suite 1

Titusville, FL 32780

(321) 264-1193

E-mail: Kevin.brown@cctcorp.com

KSC-12512



Study of Rapid-Regression Liquefying Hybrid Rocket Fuels

A report describes experiments directed toward the development of paraffin-based hybrid rocket fuels that burn at regression rates greater than those of conventional hybrid rocket fuels like hydroxyl-terminated butadiene. The basic approach followed in this development is to use materials such that a hydrodynamically unstable liquid layer forms on the melting surface of a burning fuel body. Entrainment of droplets from the liquid/gas interface can substantially increase the rate of fuel mass transfer, leading to surface regression faster than can be achieved using conventional fuels. The higher regression rate eliminates the need for the complex multi-port grain structures of conventional solid rocket fuels, making it possible to obtain acceptable performance from single-port structures. The high-regression-rate fuels contain no toxic or otherwise hazardous components and can be shipped commercially as non-hazardous commodities. Among the experi-

ments performed on these fuels were scale-up tests using gaseous oxygen. The data from these tests were found to agree with data from small-scale, low-pressure and low-mass-flux laboratory tests and to confirm the expectation that these fuels would burn at high regression rates, chamber pressures, and mass fluxes representative of full-scale rocket motors.

This work was done by Greg Zilliac and Shane DeZikwa of Ames Research Center and M. Arif Karabeyoglu, Brian J. Cantwell, and Paul Castellucci of Stanford University. Further information is contained in a TSP (see page 1).

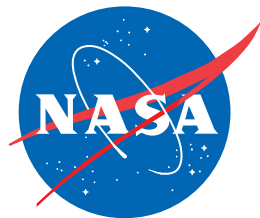
Inquiries concerning rights for the commercial use of this invention should be addressed to the Patent Counsel, Ames Research Center, (650) 604-5104. Refer to ARC-14486-2.

More About the Phase-Synchronized Enhancement Method

A report presents further details regarding the subject matter of "Phase-Synchronized Enhancement Method for Engine Diagnostics" (MFS-26435), *NASA Tech*

Briefs, Vol. 22, No. 1 (January 1998), page 54. To recapitulate: The phase-synchronized enhancement method (PSEM) involves the digital resampling of a quasi-periodic signal in synchronism with the instantaneous phase of one of its spectral components. This resampling transforms the quasi-periodic signal into a periodic one more amenable to analysis. It is particularly useful for diagnosis of a rotating machine through analysis of vibration spectra that include components at the fundamental and harmonics of a slightly fluctuating rotation frequency. The report discusses the machinery-signal-analysis problem, outlines the PSEM algorithms, presents the mathematical basis of the PSEM, and presents examples of application of the PSEM in some computational simulations.

This work was done by Jen-Yi Jong of AI Signal Research, Inc., for Marshall Space Flight Center. For further information, contact the company at asri@aisignal.com or (256) 551-0008. MFS-31409



National Aeronautics and
Space Administration